ELSEVIER

Journal of Magnetism and Magnetic Materials 225 (2001) 30–36

Journal of magnetism and magnetic materials

www.elsevier.com/locate/jmmm

Synthesis and characterization of surfactant-coated superparamagnetic monodispersed iron oxide nanoparticles

D.K. Kim[a,*], Y. Zhang[a], W. Voit[b], K.V. Rao[b], M. Muhammed[a]

[a]*Materials Chemistry Division, Royal Institute of Technology, SE-100 44 Stockholm, Sweden*
[b]*Engineering Materials Physics Division, Royal Institute of Technology, SE-100 44 Stockholm, Sweden*

Abstract

Synthesis and coating of superparamagnetic monodispersed iron oxide nanoparticles was carried out by chemical solution method. Controlled co-precipitation technique was used to prevent undesirable critical oxidation of Fe^{2+}. The obtained Fe_3O_4 nanoparticles were coated with sodium oleate. Low-field AC susceptibility and SQUID measurement show superparamagnetism with a blocking temperature around 150 K, and almost immeasurable remanence and coercivity.

Keywords: Nanoparticles; Superparamagnetism; Surfactant; Coprecipitation; Ferrofluid

1. Introduction

Recently, synthesis of magnetic materials on the nanoscale has been a field of intense study, due to the novel mesoscopic properties shown by particles of quantum dimensions located in the transition region between atoms and bulk solids. Nanosized particles have physical and chemical properties that are characteristic of neither the atom nor the bulk counterparts [1]. Quantum size effects and the large surface area of magnetic nanoparticles dramatically change some of the magnetic properties and exhibit superparamagnetic phenomena and quantum tunneling of magnetization, because each particle can be considered as a single magnetic domain. Based on their unique mesoscopic physical, tribological, thermal, and mechanical properties, superparamagnetic nanoparticles offer a high potential for several applications in different areas such as ferrofluids, color imaging, magnetic refrigeration, detoxification of biological fluids, magnetically controlled transport of anti-cancer drugs, magnetic resonance imaging contrast enhancement and magnetic cell separation [2–5].

A difficulty related to the nature of ferrofluids is that the nanoparticles, which have a large ratio of surface-area to volume, tend to agglomerate in order to reduce their surface energy (> 100 dyn/cm) by strong magnetic dipole–dipole attractions between particles. Therefore, one of the main problems in producing stable magnetic fluid is to prevent the agglomeration during the synthesis and coating process.

* Corresponding author. Tel.: +46-8-790-8148; fax: +46-8-790-9072.
E-mail address: kyung@matchem.kth.se (D.K. Kim).

0304-8853/01/$ - see front matter
PII: S0304-8853(00)01224-5

Table 1
Samples synthesized under different conditions and their average particle sizes (D); calculated from XRD, TEM and magnetization data

Sample	pH	NaOH (M)	D_{XRD} (Å)	D_{TEM} (Å)	D_{MAG} (Å)
S1	14	0.9	13	—	—
S2	14	1.0	17	—	—
S3	14	1.1	29	—	—
S4	14	1.5	30	—	—
S5	12.5	1.5	55	—	—
S6	11.54	1.5	60	72	54

2. Experimental

All the chemicals were of reagent grade used without further purifications. Ferric chloride hexahydrate ($FeCl_3 \cdot 6H_2O > 99\%$), ferrous chloride tetrahydrate ($FeCl_2 \cdot 4H_2O > 99\%$) and sodium oleate ($C_{18}H_{33}NaO_2 > 99\%$) were obtained from Aldrich while Sodium hydroxide ($NaOH > 99\%$) and hydrochloric acid ($HCl > 37\%$) from KEBO. Milli-Q water was re-deionized (specific conductance $< 0.1\,\mu s/cm$) and deoxygenated by bubbling N_2 gas for 1 h prior to the use.

Stock solutions of 1.28 M $FeCl_3 \cdot 6H_2O$, 0.64 M $FeCl_2 \cdot 4H_2O$ and 0.4 M HCl were prepared as a source of iron by dissolving the respective chemicals in Milli-Q water under vigorous stirring. In the same way, stock solutions of 0.9–1.5 M NaOH were prepared as alkali sources. A solution of 0.01 M HCl was prepared for surface neutralization, while a solution of 1.5 M sodium oleate (surfactant) at pH = 9.4 was prepared for coating.

Aqueous dispersion of magnetic nanoparticles was prepared by alkalinizing an aqueous mixture of ferric and ferrous salts with ammonia at room temperature [6]. In the present study, a solution of NaOH was used as alkali source instead of ammonia. N_2 gas was flown through the reaction medium during synthesis operation in a closed system.

25 ml of iron source was added drop-wise into 250 ml of alkali source under vigorous mechanical stirring (2000 rpm) for 30 min at room temperature.

Two operating conditions, (i) the concentration of NaOH, and (ii) the pH, were varied for different synthesis experiments as shown in Table 1. The precipitated powder was isolated by applying an external magnetic field, and the supernatant was removed from the precipitate by decantation. Deoxygenated Milli-Q water was added to wash the powder and the solution was decanted after centrifugation at 3500 rpm. After washing the powder 4 times, 0.01 M HCl was added to neutralize the anionic charge on the particle surface. The cationic colloidal particles were separated by centrifugation and peptized by adding deoxygenated Milli-Q water.

Based on the XRD results, Fe_3O_4 nanoparticles 6 nm in size (sample S6 in Table 1) were selected for coating treatment. Coating was carried out using surfactant solution under vigorous mechanical stirring for 30 min at 90°C. After coating, the surfactant adsorbed physically on the particle surface was removed by washing with deoxygenated Milli-Q water, centrifugation and peptizing the solution for three times.

All the main synthesis steps were carried out by passing N_2 gas through the solution media to avoid possible oxygen contamination during the operations. All the characterizations of the sample were done in solid phase.

The structural properties of Fe_3O_4 powders obtained were analyzed by X-ray powder diffraction (XRD) with a Philips PW 1830 diffractometer using the monochromatized X-ray beam from the nickel-filtered Cu K_α radiation. The average size of the crystals (D; Å) was estimated using Scherrer's formula [7]. The particle size and morphology were examined using a JEOL-2000EX transmission electron microscope (TEM).

The DC magnetic properties were carried out using a Quantum Design $MPMS_2$ SQUID magnetometer. The zero-field-cooled (ZFC) and field-cooled (FC) measurements were performed by

cooling the sample to 5 K at zero field or in the presence of an external field of 10 Oe, respectively. All the magnetic measurements during the warming runs were carried out in a field of 10 Oe. The hysteretic loops were measured from 5 K to room temperature. AC-magnetic measurements were also performed using a high sensitive laboratory-built two-position AC susceptometer with a three-coil mutual inductance bridge. The driving field was 10 Oe (rms) in our measurement while the frequency was varied from 1 to 1031 Hz.

The precipitated powders are black in color. The chemical reaction of Fe_3O_4 precipitation is expected as follows:

$$Fe^{2+} + 2Fe^{3+} + 8OH^- \rightarrow$$

$$Fe_3O_4\,(\text{black colloidal particles}) + 4H_2O. \quad (1)$$

According to the results of thermodynamic modeling of this system, a complete precipitation of Fe_3O_4 should be expected between pH = 7.5–14, while maintaining a molar ratio of Fe^{2+}: Fe^{3+} = 1 : 2 under a non-oxidizing environment. Otherwise, Fe_3O_4 might also be oxidized as

$$Fe_3O_4 + 0.25O_2 + 4.5H_2O \rightarrow 3Fe(OH)_3. \quad (2)$$

This would critically affect the physical and chemical properties of the nanosized magnetic particles. In order to prevent them from possible oxidation in air as well as from agglomeration, Fe_3O_4 nanoparticles produced by reaction (1) were usually coated with organic or inorganic molecules during the precipitation process. To control the reaction kinetics, which is strongly related with the oxidation speed of iron species, the present method of flowing N_2 gas is introduced to compare with already published methods [6].

The experimental results have shown that flowing N_2 gas not only protects critical oxidation but also reduces the particle size when compared with methods without removing the oxygen. For example, the particle size was reduced from 80 (in air) to 60 Å (in N_2).

Table 1 shows the average crystal sizes, measured by XRD and TEM, of Fe_3O_4 nanoparticles synthesized under different conditions. The crystal sizes determined by Scherrer's equation with XRD data have been found in a range of 13–60 Å. When

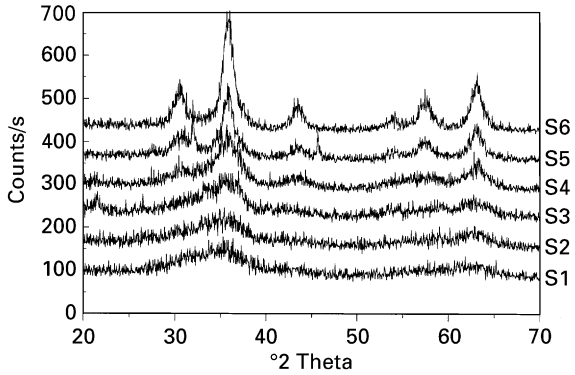

Fig. 1. X-ray powder diffraction patterns for the as-precipitated nanoparticles shown in Table 1 under different pH and NaOH concentration conditions.

the concentration of precipitating NaOH solution is increased from 0.9 to 1.5 M at pH = 14 (samples S1–S4), the crystal size is increased from 13 to 30 Å. On the other hand, the pH value of the solution for precipitation also plays an important role in controlling the crystal size. For solutions of 1.5 M NaOH (samples S4–S6), decreasing the pH value from 14 to 11.54 has resulted in increasing particle size from 30 to 60 Å.

Fig. 1 shows the XRD patterns for the as-precipitated powders of samples S1–S6. It indicates that Fe_3O_4 is the dominant phase in all the samples though a remarkable broadening of the peaks goes from sample S1 to S6. The crystallization of Fe_3O_4 nanoparticles at the most intense peak, corresponding to the (3 1 1) reflection in Fe_3O_4, is related with the mean size of the crystals according to the Scherrer equation.

The particle-size distribution and morphology were examined by TEM imaging. As shown in Fig. 2, the Fe_3O_4 powder of sample S6 consists almost of perfect single particles, though their morphology is somewhat irregularly shaped from oval to sphere. The size distribution was calculated using the following equation based on a log–normal function [9]:

$$p(d) = \frac{1}{D\sigma_d\sqrt{2\pi}} \exp\left(-\frac{1}{2\sigma_d^2} \left(\ln\frac{D}{D_0} \right)^2 \right), \quad (3)$$

where σ_d is the diameter standard deviation and D_0 is the mean diameter. These results hold for a

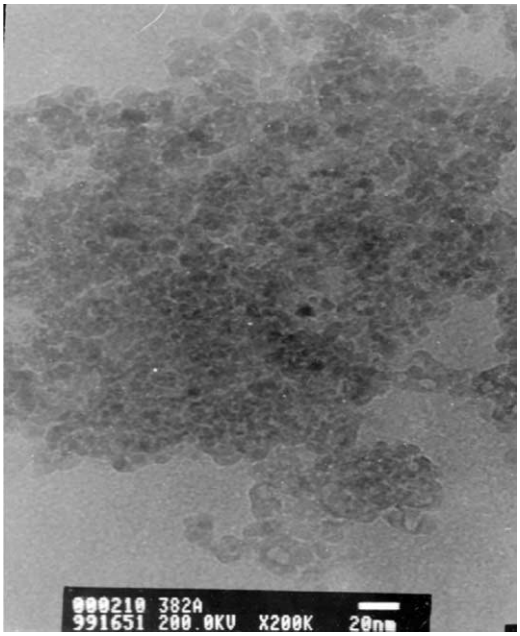

Fig. 2. TEM micrograph of Fe_3O_4 nanoparticles (sample S6, Table 1).

volumetric standard deviation $\sigma_v = 3\sigma_d$, and a mean volume $V_0 = (\pi/6)D_0^3$ particle size determined in this way is 72 Å with a standard deviation $\sigma_d = 0.2$, which is close to the crystal size calculated from XRD data (60 Å) for sample S6. This shows that the Fe_3O_4 powder of sample S6 is nanocrystalline.

The temperature dependence of magnetization (Fig. 3) of the nanoparticles exhibits a cusp around 150 K in the zero-field-cooled (ZFC) susceptibility, and a blocking temperature T_B determined from the branching of the ZFC and FC data. As it is well known, above T_B, superparamagnetic particles become thermally unstable and the magnetizations exponentially decrease as MV/KT become larger than 1. The superparamagnetic particles deflect uniquely to the strong field side of the gradient magnet, but this behavior decreases as a function of increasing temperature. When the particles are chemically coated with sodium oleate, as shown in Fig. 3 the blocking temperature is suppressed to a lower temperature. Without coating of surfactant on the particles, due to the increase in the large ratio of surface area to volume, the attractive force

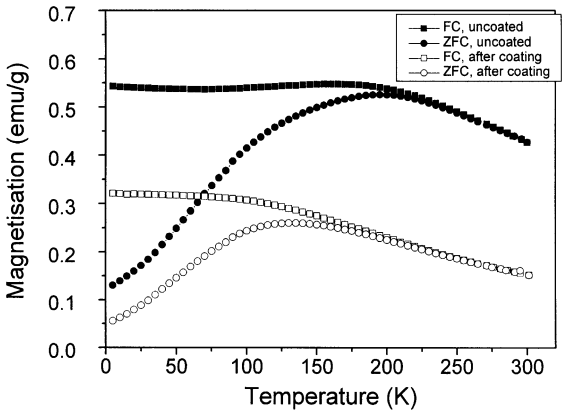

Fig. 3. Magnetization vs. temperature measured at 10 Oe in the zero-field-cooled and field-cooled states for nanoparticles (S6) before and after being coated with sodium oleate.

between the nanoparticles will increase, and agglomeration of the nanoparticles will take place, as seen in Fig. 2. These agglomerated nanoparticles act as a cluster, resulting in an increase of the blocking temperature. In contrast, the surfactant-coated nanoparticles are more freely aligned with the external field than the uncoated nanoparticles. The repulsive force between hydrophobic surfactant molecules coated on single particles can prevent them from agglomeration [10]. The total effective magnetic moment of such coated particles is found to decrease, which is most likely due to a non-collinear spin structure originated from the pinning of the surface spins and coated surfactant at the interface of nanoparticles. The measured magnetic moment is also found to decrease due to the contribution of the volume of the diamagnetic coating mass to the total sample volume.

The hysteresis loop measured from 5 to 300 K for the uncoated Fe_3O_4 nanoparticles is shown in Fig. 4. As seen in the figure, the typical characteristics of superparamagnetic behavior are observed showing almost immeasurable coercivity and remanence above the blocking temperature. The magnetization of the nanoparticles below the blocking temperature has a hysteretic feature. The magnetic particle size and size distribution can be calculated from these magnetization curves using the following formula [8]:

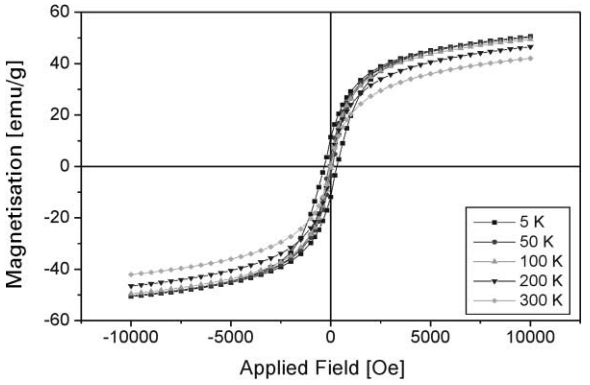

Fig. 4. Magnetization vs. applied magnetic field for nanoparticles without coating (S6).

$$D_{\mathrm{m}} = \left(\frac{18kT}{\pi}\frac{\chi_{\mathrm{i}}}{\rho M_{\mathrm{S}}^2}\right)^{1/3}. \tag{4}$$

Here, χ_{i} is the initial magnetic susceptibility $\chi_{\mathrm{i}} = (\mathrm{d}M/\mathrm{d}H)_{H\to 0}$ and ρ is the density of Fe_3O_4 (5.18 g/cm^3). The initial slope near the origin was determined from the hysteresis plots by curve-fitting the linear portion of the data. The saturation magnetization M_{S} from the magnetization curve in Fig. 4 for the uncoated Fe_3O_4 nanoparticles was found to be 42.1 emu/g at 300 K. Thus, the magnetic particle size D_{m} of sample S6 was calculated with 56 Å at 300 K. This value of D_{m} is smaller than the particle size observed from TEM measurement. The difference between D_{m} and D_{TEM} is most likely due to contributions of a magnetically "dead" layer reported to be present on the surface of particles [11].

For superparamagnetic particles, the true magnetic moment at a particular temperature can be calculated using the Langevin function [12].

$$M = M_{\mathrm{S}}\left(\coth\left(\frac{\mu H}{k_{\mathrm{b}}T}\right) - \frac{k_{\mathrm{b}}T}{\mu H}\right), \tag{5}$$

where $\mu(= M_{\mathrm{S}}\pi D^3/6)$ is the true magnetic moment of each particle, k_{b} is the Boltzmann constant, T is the absolute temperature and M_{S} is the saturation magnetization. Fig. 5 shows the best fit for the Langevin function in Eq. (5). From this data fitting, the mean-magnetic moment per particle of sample S6 is found to be $7011\mu_{\mathrm{B}}$.

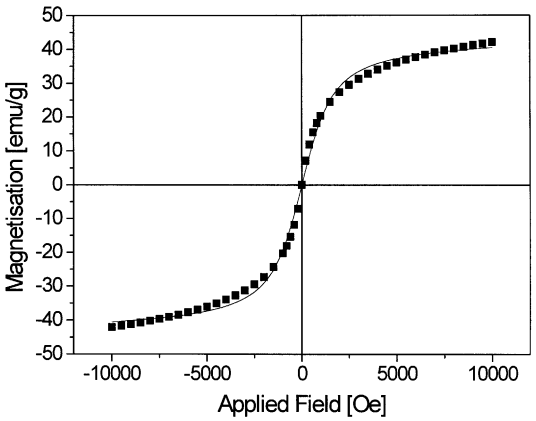

Fig. 5. Magnetization vs. applied magnetic field for nanoparticles (S6) without coating at 300 K. Experimental (solid rectangle) and calculated (solid line) data represent the best fit for the Langevin function.

The dynamics of magnetic relaxation were investigated using AC-magnetic susceptometry. For a non-interacting single particle with barrier energy E_0 and uniaxial anisotropy fluctuations, the thermal relaxation process follows the Néel–Arrhenius law [13],

$$\tau_{\mathrm{r}} = \left(\frac{1}{f_0}\right)\exp\left(\frac{E_0}{k_{\mathrm{B}}T}\right), \tag{6}$$

where τ_{r} is the relaxation time of the magnetic moment of the particle, f_0 is the attempt frequency of the transition, k_{B} is the Boltzmann constant, and T is the absolute temperature. The average energy barrier $E_0(= KV$, where K is the effective anisotropy energy constant, and V the volume of the particle) and f_0 can be directly obtained by AC-magnetic susceptometry measurements. The cusp temperature, i.e. the temperature corresponding to the maximum of the in-phase component of the AC-susceptibility, corresponds to the blocking temperature at which the relaxation time is equal to the time scale of the measurement, and can be expressed by $\tau_{\mathrm{m}} = 1/f_0$. The plot of $-\ln(f_0)$ vs. $1/T_{\mathrm{B}}$ gives a straight line with a slope E_0 and an intercept τ_{m}, as shown in Fig. 6.

When the distance between the nanoparticles is large enough, interparticle interactions between

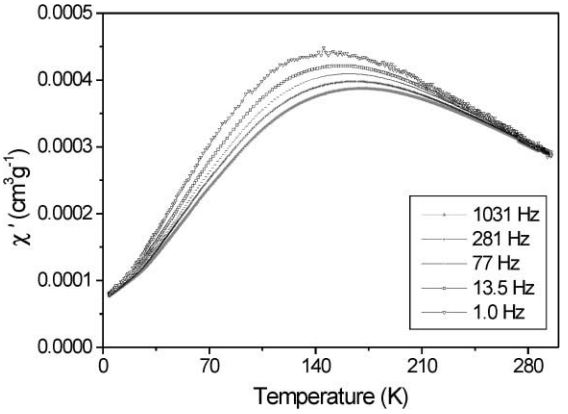

Fig. 6. AC-magnetic susceptibility data for nanoparticles (S6) coated with sodium oleate measured in the frequency range 1–1031 Hz.

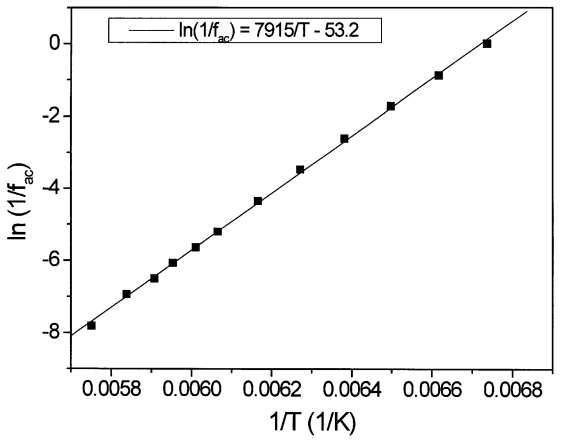

Fig. 7. Temperature dependence of the relaxation time of the magnetization estimated from AC-magnetic susceptometry data for nanoparticles (S6) coated with sodium oleate measured in the frequency range 1–1031 Hz.

dipoles are negligible. Due to superparamagnetic relaxation around the blocking temperature, at which the relaxation time τ becomes equal to zero, the anisotropy energy barrier ΔE is small enough compared to thermal energy $k_B T$, and the direction of the moment fluctuates rapidly and gives rise to thermal fluctuation between the particles. The exponential factor τ_m is usually found to be in the order of 10^{-9}–10^{-11} s for ferro- and ferrimagnetic nanoparticles. The data for the frequency-dependent susceptibility for sample S6 (shown in Fig. 7), coated with sodium oleate, show that the relaxation time follows the Néel–Arrhenius law (Eq. (6)), but with an unphysical value of $\tau_m = 7.8 \times 10^{-24}$ s. This experimental value of τ_m has been related to interparticle interaction, as the decrease in the interparticle surface area affects the anisotropy energy barrier. Therefore, on reducing the sample amount or diluting this sample in solution, a value for τ_m in the range of 10^{-9}–10^{-11} s can be expected [14].

3. Conclusion

We have presented a controlled coprecipitation method, which demonstrates the feasibility of synthesizing monocrystalline nanoparticles of Fe_3O_4 with a size of a few nanometers. The hydrosol of Fe_3O_4 nanoparticles contains no surfactant, at the first stage, and has a narrow particle-size distribution. It can be used as a source for direct incorporation with required coating materials or in the naked form for ultrathin films without requiring additional processes to remove excessive surfactants. After coating by surfactant, at the second stage, the nanoparticles can be monodispersed. These nanoparticles exhibit superparamagnetic behavior and can be useful for relevant medical and physical applications.

Acknowledgements

This work has been supported by Swedish Foundation for Strategic Research (SSF-6711) and Swedish Research Council for Engineering Sciences (TFR). It is a pleasure to acknowledge many continuous discussions with Dr. V. Ström during the magnetic measurements in this project.

References

[1] B.H. Sohn, R.E. Cohen, Chem. Mater. 9 (1997) 264.
[2] J. Popplewell, L. Sakhnini, J. Magn. Magn. Mater. 149 (1995) 72.
[3] K. Raj, B. Moskowitz, R. Casciari, J. Magn. Magn. Mater. 149 (1995) 174.

[4] R.S. Molday, D. Mackenzie, J. Immunol. Meth. 52 (1982) 353.
[5] C.W. Jung, P. Jacobs, Magn. Res. Imaging 13 (1995) 661.
[6] Y.S. Kang, S. Risbud, J.F. Rabolt, P. Stroeve, Chem. Mater. 8 (1996) 2209.
[7] R. Massart, V. Cabuil, J. Phys. Chem. 84 (1987) 967.
[8] R. Massart, IEEE Trans. Magn. MAG-17 (1981) 1247.
[9] C.G. Granqvist, R.H. Buhrman, J. Appl. Phys. 47 (1976) 2200.
[10] X.M. Lin, C.M. Sorensen, K.J. Klabunde, G.C. Hadjipanayis, Langmuir 14 (1998) 7140.
[11] R. Kaiser, G. Miskolczy, J. Appl. Phys. 41 (1970) 1064.
[12] B.D. Cullity, Introduction to Magnetic Materials, Addison-Wesley, Reading, MA, 1974, p. 94.
[13] L.A. Néel, Geophys. 5 (1949) 11.
[14] J.M. Gonzalez, M.I. Montero, J.A. Lópea-Pérez et al., IEEE Trans. Magn. 34 (1998) 2114.